J. Fluid Mech. (1978), *vol.* 84, *part* 1, *pp.* 145–165
Printed in Great Britain

Rimming flow: numerical simulation of steady, viscous, free-surface flow with surface tension

By F. M. ORR† AND L. E. SCRIVEN

Department of Chemical Engineering and Materials Science,
University of Minnesota, Minneapolis

(Received 3 November 1976)

Flow in a partly liquid-filled, rotating, horizontal cylinder is analysed by means of finite-element numerical simulation. Of alternative methods for locating the free surface, a boundary collocation scheme with Newton–Raphson iteration converges. This method forces the residual in the normal-stress boundary condition to zero at a finite set of points on the liquid meniscus. Solutions of the steady, two-dimensional, incompressible flow problem show circumferential variation of the liquid-film thickness and corresponding pressure and velocity fields, including recirculation zones. The complications of an unknown meniscus location and a nonlinear normal-stress condition when surface tension is significant are illustrated. The finite-element method proves an effective and convenient tool for such flows, in which inertial, gravitational, pressure, viscous and capillary forces are all important.

1. Introduction

Viscous liquid flows partially bounded by a free fluid interface with gas occur in endless variety. One need look only as far as coating industries to find abundant technologically important flows which challenge accurate mathematical description. There are difficulties because (i) the location of the free surface is not known *a priori*; (ii) the shape of the free surface influences the flow through a complicated nonlinear boundary condition, the normal-stress condition; (iii) there may be a stress singularity at any three-phase contact line, where a free surface intersects a solid boundary (Huh 1969; Huh & Scriven 1971). Generally some sort of iterative procedure is needed to locate the free surface, which shifts from trial to trial and rarely coincides with any convenient co-ordinate surface. Convergence of any given procedure is an open question. Nor is uniqueness of a solution obvious, as discussed by Taylor (1963). Nevertheless, approximation methods offer the main hope for solving the full flow equations in all but the very simplest of viscous free-surface flows. In this paper we report on two iterative methods for free-surface flows in which the effects of surface-tension, viscous, gravitational and inertial forces are all important. The case treated is the steady rimming flow of a liquid film inside a horizontal rotating cylinder. Various limits have been studied recently by Ruschak & Scriven (1976).

When motion is steady at a free surface between liquid and effectively inviscid, massless gas the boundary conditions are (i) no flow normal to the surface, (ii) no

† Present address: Shell Development Company, P.O. Box 481, Houston, Texas 77001.

tangential stress on the surface† and (iii) balancing of gas pressure, liquid pressure and normal viscous stress of the liquid with the capillary pressure, the latter being the product of the surface tension and mean curvature of the surface. All iterative schemes employ a similar strategy. First a location of the free surface is chosen, either by an informed guess or on the basis of the previous iterations. The Navier–Stokes and continuity equations are solved for the velocity and pressure fields in the liquid, but only two of the three boundary conditions are satisfied. The residual in the third boundary condition is then used to decide how to alter the location of the free surface, and the process is repeated to convergence – or frustration.

Iterative schemes can be classified according to which of the three boundary conditions is used as the criterion for relocating the free surface. Stream-surface schemes are those in which the kinematic boundary condition is employed, a new approximation to the position of the surface streamline being found from the velocity field determined with the preceding approximation. Normal-stress schemes are those in which the imbalance in the normal-stress boundary condition is the basis for improving the surface location. Tangential-stress schemes would be those in which the residual viscous shear stress at the boundary was used, but no scheme of this type has been reported.

Nickell, Tanner & Caswell (1974) used a stream-surface scheme to solve by the finite-element method the problem of the creeping Newtonian jet; Tanner, Nickell & Bilger (1975) extended the computation to non-Newtonian liquids. The new free surface is the streamline originating from the orifice lip at each iteration. Not described is the procedure followed when this streamline falls outside the previous one, i.e. outside the domain in which the approximate velocity field is known. Presumably this velocity field is extrapolated in some admissible way. Stream-surface schemes and the finite-element method have also been used by Thompson, Mack & Lin (1969) for slow flow of an incompressible non-Newtonian liquid and by Chan & Larock (1973) and Larock & Taylor (1976) for a potential jet. All of these investigators neglected capillary pressure. That is, the effect of surface tension was excluded.

Williamson (1970, 1972) included the effect of surface tension and employed successfully a normal-stress scheme. He studied the flow when two flexible but inextensible strips with viscous liquid between them are pulled apart as they emerge from passing between a pair of cylindrical rollers. He neglected inertial effects and solved the resulting biharmonic equation for the stream function by means of a finite-difference rather than a finite-element method. Williamson represented the entire free surface of interest by a single sixth-degree polynomial with two adjustable parameters. These were adjusted in each iteration to minimize the residual in the normal-stress boundary conditions. Details of the procedure are not reported.

Two new normal-stress schemes are described here. For the problem of rimming flow one is successful and the other is not. Both require solution of a flow problem given an estimate of the free-surface location. The solutions are generated by the finite-element method, which has advantages over other available methods, as discussed in §3. The iterative schemes and their convergence behaviour are covered in §§4 and 5 and sample numerical solutions of the rimming flow problem are presented in §6.

† The tangential stress on the surface does not vanish when there are surface-tension gradients in the surface, a possibility which is not considered here.

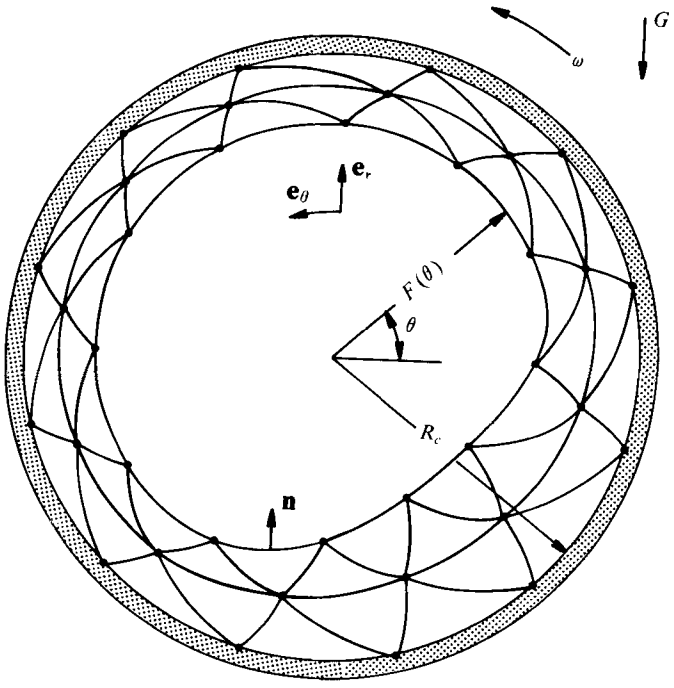

FIGURE 1. A horizontal cylinder rotates about its axis. A film of liquid of thickness $R_c - F(\theta)$ is distributed on the interior wall of the cylinder.

2. Rimming flow

Consider the flow of a liquid layer around the inside surface of a rotating horizontal drum or cylinder, as sketched in figure 1. The hollow rigid cylinder is of radius R_c and effectively infinite length. It spins about its axis with rotational speed ω. Distributed over the cylinder wall is a film of thickness $R_c - F$ of incompressible Newtonian liquid whose free surface exhibits a surface tension σ. Inside the film is a core of inviscid gas at a specified pressure P_0; the density of the gas is negligible. Only steady two-dimensional flows are considered. When the effect of the gravitational field vanishes the flow is necessarily solid-body rotation of a uniform liquid film at speed ω.

This and closely related flows are encountered in cream separators, liquid degassers, pipe coating, rotational moulding and spin casting of materials, and other applications. The case treated is a non-trivial example of a steady, two-dimensional, viscous flow with a free surface, and it has a couple of features which recommend it for testing iterative schemes for locating the free surface. First, there is neither an inflow nor an outflow boundary and so the complication of upstream and downstream boundary conditions is avoided. Second, there is no gas/liquid/solid contact line and so the danger of singularities there is avoided too.

The governing equations for the flow are

$$\nabla.(\rho\mathbf{V}\mathbf{V}+\mathbf{T})-\mathbf{G}=0, \quad \nabla.\mathbf{V}=0 \quad \text{in } D, \tag{2.1}$$

$$\mathbf{T}=P\mathbf{I}-\mu[\nabla\mathbf{V}+(\nabla\mathbf{V})^{\mathrm{T}}] \tag{2.2}$$

($\mathbf{T}$ is the stress tensor, $\mathbf{I}$ the unit tensor). The flow domain D is $F(\theta) \leqslant R \leqslant R_c$, $0 \leqslant \theta \leqslant 2\pi$. The pressure and velocity are used rather than the stream function and

vorticity because the form of the normal-stress boundary condition makes it useful to have the pressure available explicitly.

Convenient dimensionless variables are

$$r \equiv R/R_c, \quad \mathbf{v} \equiv \mathbf{V}/\omega R_c, \quad p \equiv (P-P_0)/\rho\omega^2 R_c^2, \quad f \equiv F/R_c. \tag{2.3}$$

Appropriate dimensionless parameters are a Reynolds number Re, a Weber number s and a dimensionless gravity g:

$$Re \equiv \rho\omega R_c^2/\mu, \quad s \equiv \sigma/\rho\omega^2 R_c^3, \quad g \equiv G/\omega^2 R_c. \tag{2.4}$$

The governing equations become

$$\nabla.(\mathbf{vv}+\boldsymbol{\tau})-g\mathbf{j} = 0, \quad \nabla.\mathbf{v} = 0, \tag{2.5}$$

where

$$\tau = p\mathbf{I} - Re^{-1}[\nabla\mathbf{v}+(\nabla\mathbf{v})^{\mathrm{T}}]$$

and, in cylindrical polar co-ordinates,

$$\nabla = \mathbf{e}_r\partial/\partial r + \mathbf{e}_\theta r^{-1}\partial/\partial\theta.$$

The boundary conditions are the adherence condition on the rigid cylinder

$$\mathbf{v} = \mathbf{e}_\theta \quad \text{on} \quad r = 1, \tag{2.6}$$

the traction conditions

$$\mathbf{nn}:\boldsymbol{\tau}+2Hs = 0, \quad \mathbf{tn}:\boldsymbol{\tau} = 0 \quad \text{on} \quad r = f(\theta) \tag{2.7}$$

and the kinematic condition

$$\mathbf{n}.\mathbf{v} = 0 \quad \text{on} \quad r = f(\theta). \tag{2.8}$$

The unit normal and tangent to the free-surface are given by

$$\mathbf{n} = -\frac{f\mathbf{e}_r + f_\theta\mathbf{e}_\theta}{(f^2+f_\theta^2)^{\frac{1}{2}}}, \quad \mathbf{t} = \frac{f_\theta\mathbf{e}_r - f\mathbf{e}_\theta}{(f^2+f_\theta^2)^{\frac{1}{2}}}. \tag{2.9}$$

Because the flow is incompressible the free-surface location must satisfy the constraint that the volume of liquid (and hence the volume of gas) remains constant:

$$f_0 = \frac{1}{2\pi}\int_0^{2\pi} f^2(\theta)\,d\theta. \tag{2.10}$$

Finally, all of the variables are periodic with period 2π, i.e.

$$\mathbf{v}(r,\theta) = \mathbf{v}(r,\theta+2\pi), \quad p(r,\theta) = p(r,\theta+2\pi), \quad f(\theta) = f(\theta+2\pi), \tag{2.11}$$

as are all derivatives of these variables.

The integral constraint (2.10) sets the level of pressure in the flow field. Without it, the pressure is determined only up to a constant since it appears only in natural boundary conditions.

A number of simplified versions of this problem have been solved. Phillips (1960) found perturbations about the zero-gravity solution but neglected the contributions of viscosity and surface tension. Cerro & Dieber (1976) solved a boundary-layer approximation but also neglected surface tension. Ruschak & Scriven (1976) included surface tension in their perturbation analysis for small gravity though the solution at first order in gravity is not influenced by surface tension (see also Ruschak 1974). Greenspan (1976) also used perturbation methods, and studied an interesting variant of this problem in which the gas core is replaced by a weightless rigid cylinder.

3. Finite-element formulation

In the finite-element method, the flow domain is divided into geometrically simple subdomains (usually triangles or quadrilaterals) and the solution is sought as an expansion in terms of polynomial trial functions of low order which are defined within neighbouring subdomains (elements) and vanish elsewhere. The trial functions are so chosen that the expansion coefficients retain physical significance: the coefficients are the values of the dependent variables (and also their derivatives in more elaborate versions) at the vertices of the elements. The unknown coefficients in the expansions are chosen to force to zero a set of weighted residual integrals in which the trial functions are also used as the weighting functions, a Galerkin technique. Typically, an integration by parts is performed which casts some of the derivatives of the differential operator off onto the weighting functions; in the same manipulation the boundary conditions enter via an application of the divergence theorem.

The finite-element method has aspects which suit it well to the problems considered here. First, the elements need not have uniform size and shape, so that irregular domains, those bounded by other than co-ordinate surfaces, require no special handling, a significant advantage for free-surface flow problems, which by their nature occur on irregular domains. In addition, the fact that element sizes need not be uniform means that computational power can be deployed efficiently by using small elements in regions of rapid variation, within boundary layers for instance, and large ones elsewhere. Second, boundary conditions which are natural conditions for the differential operator enter into the finite-element approximations in a particularly simple way. Separately constructed approximations to such boundary conditions are not required as they are in finite-difference methods. An added advantage is that singular trial functions can easily be used in the finite-element method when the problem solution is itself singular. Singularities can arise in solutions of the Navier–Stokes equation at a three-phase contact line (Huh 1969; Huh & Scriven 1971; Ruschak 1974; Dussan V. & Davis 1974). The price to be paid for these advantages is the complexity of the resulting computer programs, which are substantially more difficult to develop than corresponding finite-difference programs.

The approximate solutions for the velocity and pressure fields are sought as expansions in a set of trial functions $\phi_j(r,\theta)$ which in the eth element take the form

$$u = \sum_{j=1}^{m} u_j \phi_j^{(e)}, \quad v = \sum_{j=1}^{m} v_j \phi_j^{(e)}, \quad p = \sum_{j=1}^{m} p_j \phi_j^{(e)}, \tag{3.1}$$

where u and v are the velocities in the r and θ directions, respectively. These expansions are substituted into the momentum and continuity equations; the expansion coefficients u_j, v_j and p_j are selected to make the resulting residuals in the differential equations orthogonal to each of the trial functions. The weighted residual integrals for (2.1) are

$$\left.\begin{aligned} \int_D \{\phi_i \nabla . (\mathbf{vv} + \boldsymbol{\tau}) - \phi_i g \mathbf{j}\}\, da = 0, \\ \int_D \phi_i \nabla . \mathbf{v}\, da = 0, \end{aligned}\right\} \quad i = 1, 2, \ldots, Q. \tag{3.2}$$

Integration by parts and the divergence theorem give

$$\left.\begin{aligned} -\int_D \{\nabla\phi_i . (\mathbf{vv}+\boldsymbol{\tau}) + \phi_i g\mathbf{j}\}\, da + \int_{\partial D} \phi_i \mathbf{n} . (\mathbf{vv}+\boldsymbol{\tau})\, ds = 0, \\ \int_D -\nabla\phi_i . \mathbf{v}\, da + \int_{\partial D} \phi_i \mathbf{n} . \mathbf{v}\, ds = 0, \end{aligned}\right\} \quad i = 1, 2, \ldots, Q, \tag{3.3}$$

where $\mathbf{n} = \mathbf{e}_r$ on the cylinder surface and $\mathbf{n}$ is given by (2.9) on the free surface. On both the solid and the free boundary $\mathbf{n} . \mathbf{v} = 0$. The stress on the free surface has only normal components. Thus $\mathbf{n} . \boldsymbol{\tau} = (\mathbf{nn}:\boldsymbol{\tau})\mathbf{n}$, and the final form of the finite-element analogue of the Navier–Stokes and continuity equations is

$$\left.\begin{aligned} \mathbf{M}_i = \int_D \{\nabla\phi_i . (\mathbf{vv}+\boldsymbol{\tau}) + \phi_i g\mathbf{j}\}\, da - \int_{\partial D_s} \phi_i (\mathbf{nn}:\boldsymbol{\tau})\, \mathbf{n} ds - \int_{\partial D_c} \phi_i \mathbf{n}_c . \boldsymbol{\tau} ds = 0, \\ C_i = \int_D \nabla\phi_i . \mathbf{v}\, da = 0, \end{aligned}\right\} \quad i = 1, 2, \ldots, Q, \tag{3.4}$$

where ∂D_s is the free surface, ∂D_c the cylinder surface and $\mathbf{n}_c = \mathbf{e}_r$ the normal to ∂D_c. The integrals are evaluated numerically by a seven-point Gaussian quadrature formula for a two-dimensional triangular simplex given by Stroud (1971, p. 314).

Equations (3.4) are nonlinear in the expansion coefficients for u and v; hence some sort of iterative solution is required. Oden (1972) reviewed the many methods which can be applied to finite elements. One of the most common is the Newton–Raphson method: the solution α to a set of nonlinear equations of the form

$$H_i(\alpha_j) = 0, \quad i, j = 1, \ldots, Q,$$

is approximated as

$$\alpha^{(k+1)} = \alpha^{(k)} - [J_{ij}^{(k)}]^{-1}\, \mathbf{H}(\alpha^{(k)}),$$

where $[J_{ij}^{(k)}]$ is the Jacobian matrix with entries

$$J_{ij}^{(k)} = [\partial H_i / \partial \alpha_j]_{\alpha=\alpha^{(k)}}.$$

Much effort has been devoted to the development of effective elements and trial functions, and there are many possible choices. Strang & Fix (1973) discuss many of the more popular elements. The simplest combination, triangles with linear trial functions, could be used for the rimming flow problem, but more complicated, higher-order trial functions bring benefits which are useful for this type of problem: (i) derivatives of the approximate solution become more accurate as the degree of the polynomial trial functions increases and (ii) element boundaries can be bent to follow a curved boundary more closely. Indeed, the velocity expansions must be differentiated to yield stress data for the free-surface location part of the algorithm; and the free surface is rarely a co-ordinate surface, so that elements which can follow the more complicated free-surface shape are worthwhile. Such features are not cost free. The bandwidth of the Jacobian matrix increases rapidly as the degree of the trial functions increases. The nonlinear transformations which bend element boundaries decrease the accuracy of the numerical integration slightly. The optimal choice of trial functions and elements is a large subject in itself, and there is no clear indication, so far, of a *best* combination.

One choice which adapts well to the requirements of the rimming flow problem is the Hermite cubic triangular element of Zlámal (1970, 1973*a*, *b*). The trial functions are cubic polynomials of the form†

$$\phi_i^{(e)} = a_{i1} + a_{i2}r + a_{i3}\theta + a_{i4}r^2 + a_{i5}r\theta + a_{i6}\theta^2 + a_{i7}r^3 + a_{i8}r^2\theta + a_{i9}r\theta^2 + a_{i10}\theta^3. \quad (3.5)$$

There are three such functions associated with each node; they are chosen to have the properties that

$$\left.\begin{aligned} &\phi_i^{(1)}(r_j,\theta_j) = \delta_{ij}, \quad \phi_i^{(2)}(r_j,\theta_j) = 0, \quad \phi_i^{(3)}(r_j,\theta_j) = 0, \\ &\frac{\partial\phi_i^{(1)}}{\partial r}(r_j,\theta_j) = 0, \quad \frac{\partial\phi_i^{(2)}}{\partial r}(r_j,\theta_j) = \delta_{ij}, \quad \frac{\partial\phi_i^{(3)}}{\partial r}(r_j,\theta_j) = 0, \\ &\frac{\partial\phi_i^{(1)}}{\partial\theta}(r_j,\theta_j) = 0, \quad \frac{\partial\phi_i^{(2)}}{\partial\theta}(r_j,\theta_j) = 0, \quad \frac{\partial\phi_i^{(3)}}{\partial\theta}(r_j,\theta_j) = \delta_{ij}. \end{aligned}\right\} \quad (3.6)$$

A tenth condition is required to specify the polynomial (3.5) uniquely. Zlámal (1970) requires that the trial function should reduce to a quadratic along the line connecting node 1 of the triangle with the centroid of the element.

The expansion of a particular variable, say p, in the eth element is

$$p^{(e)} = \sum_{i=1}^{3}\sum_{j=1}^{3} p_i^{(j)}\phi_i^{(j)}(r,\theta). \quad (3.7)$$

The expansion coefficients $p_i^{(j)}$ are the values of p and its r and θ partial derivatives at the three nodes of the triangle: $p_1^{(1)}$ is the pressure at node 1, $p_1^{(2)}$ is $\partial p/\partial r$ at node 1, $p_1^{(3)}$ is $\partial p/\partial\theta$ at node 1, and so on. These trial functions have continuous first derivatives at the nodes but not along element boundaries.

It should be noted that the same basis functions are used here for both the pressure and the velocity field. This choice simplifies programming. More important, it ensures that the cubic transformations used to follow the free surface, which are chosen to be consistent with the cubic polynomial expansion of the free-surface position (see §4), are isoparametric with all of the trial-function expansions employed in the problem. In addition, the radial derivative of the pressure on the free surface, needed in one of the surface finding schemes, is readily available.

4. Two normal-stress schemes

Iterative schemes which employ the residual in the normal-stress boundary condition, rather than that in the kinematic condition, as the criterion for adjusting the location of the free boundary appear quite likely to converge when surface tension is important. The reason is that in this type of scheme the kinematic and tangential-stress boundary conditions, which depend on surface orientation but not curvature, are imposed while the normal-stress boundary condition is not. The normal-stress condition depends on the mean curvature of the surface, which depends on second derivatives of surface position, and is therefore least accurately known of the three conditions at any given state of a numerical solution.

† For elements on the free surface, the trial functions differ slightly because cubic transformations are used to distort surface elements to follow the surface shape more closely (Zlámal 1973*a*, *b*; Orr 1976).

Both of the iterative schemes discussed below require a representation of the free surface, which for the rimming flow problem is a function of θ only. Expansions of the surface position in finite-element trial functions have proved capable of conveniently representing complicated menisci (Orr, Scriven & Rivas 1975; Orr 1976; Orr, Brown & Scriven 1976). So we seek to find the expansion coefficients α_j in

$$f(\theta) \approx \sum_{j=1}^{Q_s} \alpha_j \phi_j(\theta), \tag{4.1}$$

where Q_s is the number of trial functions in the expansion. Because second derivatives of the expansions are needed, functions of higher than first order are needed. Hermite cubic functions prove to be convenient; they have continuous first derivatives but only piecewise-continuous second derivatives. There are two trial functions associated with the ith node on the free surface, both cubic polynomials in θ:

$$\phi_i^{(k)} = a_{i1}^{(k)} + a_{i2}^{(k)}\theta + a_{i3}^{(k)}\theta^2 + a_{i4}^{(k)}\theta^3, \quad i = 1, 2, \ldots, Q_s, \quad k = 1, 2. \tag{4.2}$$

The coefficients in the trial function are so determined that

$$\phi_i^{(1)}(\theta_j) = \delta_{ij}, \quad \phi_i^{(2)}(\theta_j) = 0, \quad \frac{d\phi_i^{(1)}}{d\theta}(\theta_j) = 0, \quad \frac{d\phi_i^{(2)}}{d\theta}(\theta_j) = \delta_{ij}. \tag{4.3}$$

The trial-function expansion in the eth element for $f(\theta)$ is then

$$f(\theta) \approx \sum_{i=1}^{2} \sum_{j=1}^{2} f_i^{(j)} \phi_i^{(j)}(\theta). \tag{4.4}$$

As before, the expansion coefficients $f_i^{(j)}$ retain physical significance: $f_i^{(1)}$ and $f_i^{(2)}$ are the approximate values of f and $df/d\theta$ at $\theta = \theta_i$.

Scheme I: *boundary collocation with Newton–Raphson iteration*

In terms of the location of the free surface $f(\theta)$ the normal-stress boundary condition (2.7) is

$$\frac{f^2 + 2f_\theta^2 - ff_{\theta\theta}}{[f^2 + f_\theta^2]^{\frac{3}{2}}} - \frac{f^2}{f^2 + f_\theta^2}\left(a - b\frac{f_\theta}{f} - c\frac{f_\theta}{f^2} + d\frac{f_\theta^2}{f^3}\right) + \frac{p}{s} = 0, \tag{4.5}$$

where

$$a \equiv \frac{2}{sRe}\frac{\partial u}{\partial r}, \quad b \equiv \frac{2}{sRe}\frac{\partial v}{\partial r}, \quad c \equiv \frac{2}{sRe}\left(\frac{\partial u}{\partial \theta} - v\right), \quad d \equiv \frac{2}{sRe}\left(\frac{\partial v}{\partial \theta} + u\right).$$

The correct location of the free surface is that for which (4.5) is satisfied, though, of course, the pressure p and the coefficients a, b, c and d from the stress tensor couple the surface location to the flow field problem. Given a location of the free surface and a corresponding solution for the velocity and pressure fields the residual in (4.5) can be evaluated. In a standard collocation method the residuals are algebraic functions of the expansion coefficients. Therefore selection of the coefficients reduces to the problem of solving the nonlinear set of algebraic equations. The situation here is more complicated because the dependence of the pressures, velocities and velocity derivatives in (4.5) is through solutions to the Navier–Stokes equations rather than through an explicit functional form. In addition, the free-surface expansion must satisfy the volume constraint (2.10). If a Newton–Raphson method is to be used, the Jacobian

matrix of derivatives of the boundary residuals must be computed. A forward-difference formula (Oden 1972, p. 283) is used here to estimate those derivatives by perturbing each of the expansion coefficients in turn:

$$\partial B_i/\partial \alpha_j \approx h^{-1}[B_i(\alpha_1, \alpha_2 \ldots, \alpha_j + h, \ldots \alpha_n) - B_i(\alpha_1, \alpha_2 \ldots, \alpha_n)], \tag{4.6}$$

where B_i is the value of the boundary residual at the ith collocation point. Then the Newton–Raphson iteration takes the form

$$\boldsymbol{\alpha}^{(k+1)} = \boldsymbol{\alpha}^{(k)} - [\partial B_i/\partial \alpha_j]^{-1}\,\mathbf{B}, \tag{4.7}$$

where $\mathbf{B}$ is the vector of the normal-stress residuals evaluated at the Q_s collocation points, plus the residual in the volume constraint (2.10), and $\boldsymbol{\alpha}$ is the vector of the Q_s expansion coefficients for the free surface, plus the pressure to be specified at a datum point in the flow field. In order to have Q_s collocation points on the free surface two collocation points per element are required. The work of Douglas & Dupont (1973) suggests that the Gauss points in each element yield better accuracy than other choices of collocation points, and so Gauss points are used here. Because construction of the free-surface Jacobian matrix $[\partial B_i/\partial \alpha_j]$ is the most time-consuming step of the computation, it is reasonable to recompute that matrix only if the (Euclidean) norm of the boundary residual vector does not decrease from one iteration to the next. This constitutes a modified Newton's method (Oden 1972, p. 280). Thus the algorithm for scheme I is as follows.

(1) Guess a set of free-surface expansion coefficients.

(2) Evaluate the Jacobian matrix for the flow field problem. Guess the pressure at one node and solve (2.5) for new velocities and pressures, imposing only the kinematic and tangential-stress conditions on the free surface.

(3) Compute $\|\mathbf{B}\|$, the normal-stress residuals at the Q_s collocation points and the volume-constraint residual.

(4) If $\|\mathbf{B}\|$ has increased from the previous iteration (or if this is the first iteration) compute the surface Jacobian matrix $[\partial B_i/\partial \alpha_j]$.

(5) Calculate a new surface-location expansion from (4.7).

(6) If the change in surface location is above tolerance go to (2).

The general surface representation and the systematic procedure for improving the approximation of the free-surface location make this scheme applicable to a much broader class of free-surface flow problems than Williamson's device, which is the only other approach by way of the normal-stress residual.

Scheme II: *finite-element solution of a modified Laplace–Young equation*

The normal-stress boundary condition (2.7) is a generalization of the Laplace–Young equation of capillary hydrostatics, which balances capillary pressure with the jump in hydrostatic pressure across a curved meniscus. Efficient methods have been developed for solving the Laplace–Young equation (e.g. Huh 1969; Orr *et al.* 1975). Liquid flowing beneath the free surface adds viscous stresses and a more complicated pressure field to the usual hydrostatic pressure distribution. Thus an alternative procedure for finding the free surface is to solve the modified Laplace–Young equation in which the normal stress at the free surface is given by the flow solution from the previous iteration. The algorithm for scheme II is as follows.

(1) Guess a set of free-surface expansion coefficients and a pressure for a datum point in the flow field.

(2) Solve the momentum and continuity equations (2.5) for new velocity and pressure fields, imposing only the tangential-stress and kinematic boundary conditions.

(3) Solve (4.5) for a new location of the free surface using the values of a, b, c and d evaluated from the velocities and pressures at the previous free-surface position.

(4) Check the integral constraint (2.10). If the residual is sufficiently small go to (2) and repeat (2)–(4) to convergence. Otherwise adjust the guess for the pressure at the datum point and go to (3).

This scheme generates successive approximations to the location of the free surface. The one-dimensional finite-element method which is used here to solve (4.5) selects a surface shape which makes the residual in the normal-stress condition zero on the average over the surface. It does this for the stress field at the free surface which resulted from the flow solution for the previous free-surface location.

The weighted residual integrals for (4.5) are constructed just as in §3, except that in applying the divergence theorem the curvature of the surface over which the integration is performed has to be taken into account (Weatherburn 1939, p. 238). The resulting weighted residual integrals are

$$\int_0^{2\pi} \left[\frac{\phi_j(1-y^2)+y\phi_j'}{f(1+y^2)^{\frac{1}{2}}} - \frac{\phi_j[a-b-(c/f)y+(d/f)y^2]}{1+y^2} + \frac{\phi_j p}{s} \right] d\theta = 0, \quad j = 1, 2, \ldots, Q_s, \tag{4.8}$$

where $y = f_\theta/f$. The nonlinear equations (4.8) can be solved by a Newton–Raphson method which parallels (3.9).

The components of the stress at the free surface, a, b, c and d, are treated as constants in (4.8). They are nevertheless dependent on the position of the free surface, and the consequences of this dependence are clarified by the asymptotic expansion of the normal-stress boundary condition for small gravity (Ruschak 1974; Ruschak & Scriven 1976). Expansions of each of the dependent variables as power series in the small parameter g are constructed:

$$\left.\begin{aligned} f &\approx f_0+f_1g+f_2g^2+\ldots, \quad p \approx p_0+p_1g+p_2g^2+\ldots, \\ u &\approx u_0+u_1g+u_2g^2+\ldots, \quad v \approx v_0+v_1g+v_2g^2+\ldots. \end{aligned}\right\} \tag{4.9}$$

The solution for zero gravity is just solid-body rotation:

$$p_0 = \tfrac{1}{2}(r^2-f_0^2) - s/f_0, \quad u_0 = 0, \quad v_0 = r, \tag{4.10}$$

where f_0 is a constant set by the volume of liquid. Substitution of the expansions (4.9) into the normal-stress boundary condition (4.5) yields the equation at first order for f_1:

$$f_1''+f_1+\frac{2f_0^2}{sRe}\frac{\partial u_1}{\partial r} - \frac{p_1 f_0^2}{s} = 0, \tag{4.11}$$

where p_1 and $\partial u_1/\partial r$ are, in this iterative scheme, obtained from the flow field solution for $f(\theta) = f_0$. The solution to (4.11) is

$$f_1 = \int_0^\theta \sin(\theta-\xi)\, q(\xi)\, d\xi + \alpha \sin\theta + \beta\cos\theta, \tag{4.12}$$

where α and β are constants and

$$q(\theta) = \frac{f_0^2}{s} p_1\Big|_{r=f_0} - \frac{2f_0^2}{sRe}\frac{\partial u_1}{\partial r}\Big|_{r=f_0}.$$

The solution must satisfy the orthogonality conditions

$$\int_0^{2\pi} \sin\xi q(\xi)d\xi = 0, \quad \int_0^{2\pi} \cos\xi q(\xi)d\xi = 0, \tag{4.13}$$

which arise from the periodicity requirements on f and its first derivative. The solutions for p_1 and u_1 were found by Ruschak (1974) to be

$$p_1(r,\theta) = \mathrm{Re}[k_1(r)e^{i\theta}], \quad u_1(r,\theta) = \mathrm{Re}[k_2(r)e^{i\theta}], \tag{4.14}$$

where $k_1(r)$ and $k_2(r)$ are complex functions of r. The orthogonality conditions (4.13) are clearly violated by $q(\theta)$, which can contain no component of $\sin\theta$ or $\cos\theta$ if there is to exist a solution for f_1. Thus the iterative scheme inherent in (4.8) is not well posed: there is no solution for f_1 with the data from the flow problem at first order.

If, however, the expansions (4.9) are modified to include a dependence on the location of the free surface they become

$$\left.\begin{aligned} f &\approx f_0 + f_1 g + \ldots, \\ p &\approx p_0 + p_1 g + f_1 g[\partial p_0/\partial r]_{r=f_0} + \ldots, \end{aligned}\right\} \tag{4.15}$$

and so on. The only additional term which survives at first order comes from the pressure expansion, so that (4.11) takes the form

$$f_1'' + (1-\delta)f_1 = \tilde{q}(\theta), \tag{4.16}$$

where

$$\delta = \frac{f_0^3}{s}, \quad \tilde{q}(\theta) = \frac{f_0^2}{s} p_1\Big|_{r=f_0} - \frac{2f_0^2}{sRe}\frac{\partial u_1}{\partial r}\Big|_{r=f_i}.$$

This problem has the solution

$$f_1 = \int_0^{\theta} \sin[(1-\delta)^{\frac{1}{2}}(\theta-\xi)]q(\xi)d\xi \tag{4.17}$$

with the orthogonality conditions

$$\left.\begin{aligned} \int_0^{2\pi} \sin[(1-\delta)^{\frac{1}{2}}(2\pi-\xi)]q(\xi)d\xi = 0, \\ \int_0^{2\pi} \cos[(1-\delta)^{\frac{1}{2}}(2\pi-\xi)]q(\xi)d\xi = 0. \end{aligned}\right\} \tag{4.18}$$

Since the functions $\sin\theta$ and $\cos\theta$ do not lie in the null space of the operator in (4.14) the orthogonality conditions do not automatically rule out the existence of solutions as they did above.

Thus (4.8) must be modified by the substitution of an expansion for the pressure in the surface location for what was previously just the pressure at the previous location of the surface f_p, i.e.

$$p \approx p\Big|_{r=f_p} + (f-f_p)\frac{\partial p}{\partial r}\Big|_{r=f_p}. \tag{4.19}$$

Numerical calculations with (4.8) as originally derived completely confirm the prediction that no solution exists. The linearized set of equations is inconsistent when stress data from the flow field calculation are used to find new expansion coefficients for the free surface. The substitution of (4.19) for the pressure in (4.8) yields solutions with no difficulty, however.

5. Convergence behaviour

Solutions to the flow problem depend on four parameters: the Reynolds number Re, the dimensionless surface tension or Weber number s, the dimensionless gravity parameter or inverse rotational Froude number g, and the liquid loading, which is set by the average surface radius f_0. Since the solution at zero gravity is known, the gravity parameter is an obvious choice as an imbedding parameter; for small increments in the gravity parameter the solution should be close to that for the previous value of the gravity. The Reynolds number also can be used as an imbedding parameter, though the appropriate size of Reynolds number increments depends strongly on the size of the gravity parameter.

In our experience scheme I generated convergent solutions for all cases attempted (see §6), even when the initial boundary residual vector seemed large, i.e. the initial guess was poor. Usually three to five iterations were sufficient to reduce the maximum correction to any of the free-surface expansion coefficients to less than 10^{-5}.

On the other hand, scheme II did not yield convergent solutions except in one very special case: for $g = 0$ the solid-body-rotation solution was obtained if the initial guess for the surface was a circle centred at the origin; for other guesses the computation diverged even at zero gravity. The divergent behaviour was also observed when the initial guess for the location of the free surface seemed very good. For instance, the solid-body-rotation solution was used as a guess for the solution at $g = 10^{-6}$. At such low gravity the initial guess is very close to the true solution yet the iterative process fails to converge.

The reason almost certainly lies in the sensitivity of the pressure field to the surface location, which in turn is highly responsive to the pressure field through the normal-stress boundary condition (4.5). At each iteration the 'correction' to the free-surface position causes changes in the pressure and velocity fields which then cause larger alterations in the free-surface position. Another manifestation of the same basic issue is the necessity of expanding the pressure field in the surface location before any surface solution can be found, as discussed in the preceding section.

For the rimming flow problem scheme I converges whereas scheme II does not. The difference between the two is plain. The second selects a new surface location which balances normal stresses obtained from the current flow solution, which is in turn based on the current location of the free surface; but this method contains no measure of whether the new solution will actually reduce the imbalance in normal stress. Scheme I uses not only the imbalance in normal stresses but also estimates how that imbalance varies with surface location. Thus it demands substantially more data about the behaviour of the residual in the normal-stress boundary condition, and the additional information is sufficient to produce convergence.

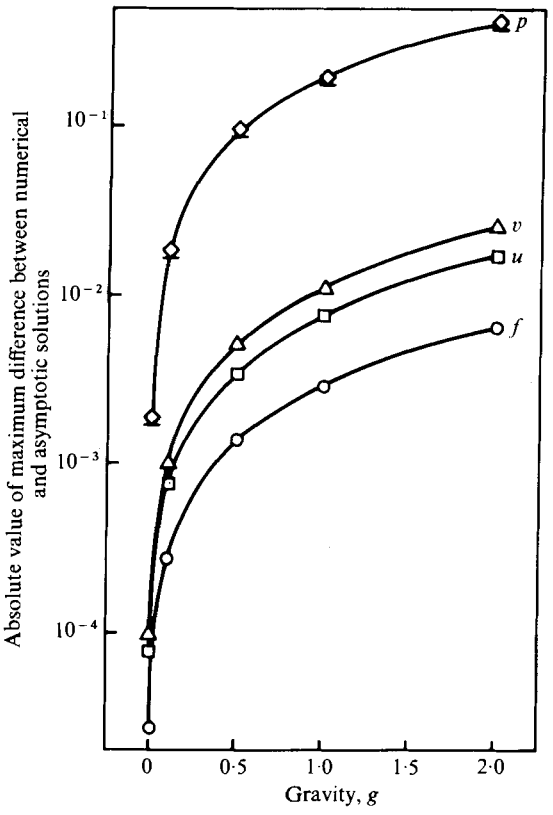

FIGURE 2. Convergence of the numerical solutions to the asymptotic solutions for small gravity ($g \to 0$) when $Re = 1$, $s = 1$ and $f_0 = 0{\cdot}5$. Asymptotic solutions of Ruschak & Scriven (1976).

6. Results of numerical simulation

Accuracy

The obvious first test of the computer program (RIMFLOW) developed as described above is whether it accurately reproduces the solid-body-rotation solution when the gravity parameter is zero. For a mesh of twelve nodes in the θ direction and only two in the r direction and parameter values $Re = 1$, $s = 1$ and $f_0 = 0{\cdot}7$, RIMFLOW produces velocities and a pressure which deviate from their exact values by about 1×10^{-5} and 6×10^{-5} respectively. The solid-body-rotation solution can be represented exactly with the Hermite cubic trial functions. Therefore at zero gravity there is no interpolation error at all. Moreover, the polar co-ordinate elements represent the zero-gravity domain exactly. The only remaining source of error is the numerical integration step. It is not exact because the functions $\sin\theta$ and $\cos\theta$ appear in the weighted residual integrals.

An additional test is provided by the asymptotic solutions for small gravity (Ruschak & Scriven 1976). That the finite-element numerical solutions agree very well with the asymptotic expansions is illustrated by figure 2. At $g = 0{\cdot}01$ the solutions for the free-surface location and radial velocity differ only in the fifth decimal while azimuthal velocities differ by less than 0·0001. The pressures differ by about 0·002.

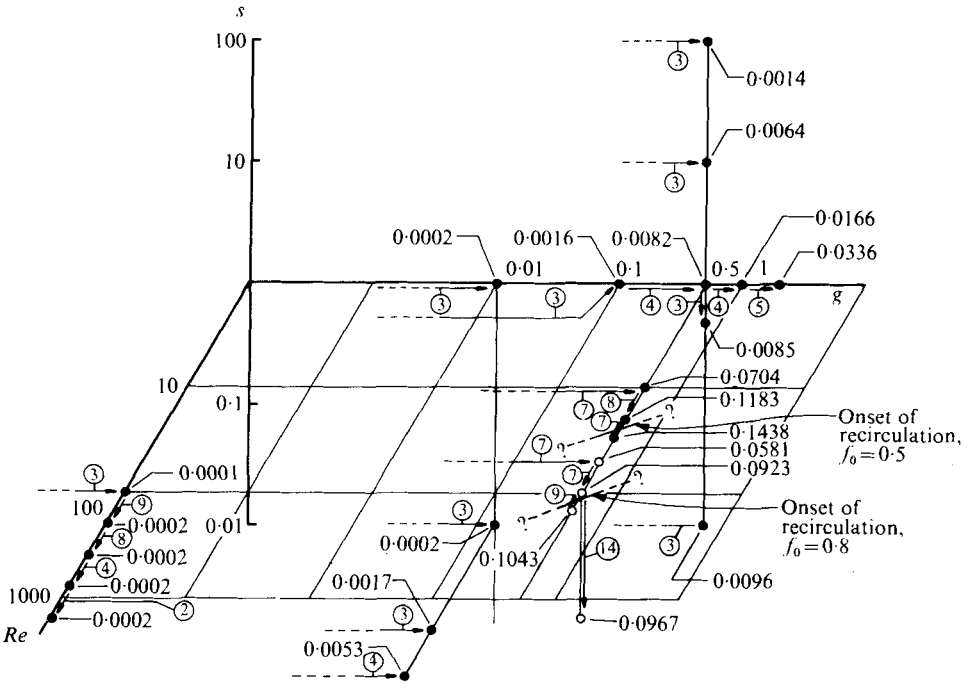

FIGURE 3. Parameter space in which rimming flow solutions were found (see text). ●, average film radius $f_0 = 0{\cdot}5$; ○, $f_0 = 0{\cdot}8$. Arrows indicate the initial guess used; broken arrow shafts denote that solid-body rotation was guessed. Circled numbers are the numbers of iterations required to reduce corrections to the surface position to less than 10^{-5}. The decimal numbers are the maximum deviation of the free surface from the average film radius, i.e. $|f - f_0|$.

Evidently the pressures produced by the finite-element program are somewhat less accurate than the velocities and the surface location. This agrees with the results of Hood & Taylor (1974), who found that the pressure field was less accurately represented than the velocity fields in a confined flow problem where the same trial-function expansions were used for both velocities and pressure. Use of lower-order basis functions for the pressure field yields more accurate pressure values but the continuity equation is less accurately satisfied. A satisfactory explanation for this behaviour has not yet been given.

What is remarkable is the agreement between the numerical and asymptotic solutions when the gravity parameter is not small. Even for $g = 2{\cdot}0$ the free-surface locations differ only in the third decimal. Ruschak's solutions at first order in gravity are quite accurate for the parameter set shown in figure 2. At higher Reynolds number, however, the agreement deteriorates more rapidly with increasing gravity.

The accuracy of the solutions which deviate substantially from solid-body rotation has not been established. Further refinement of the fairly crude meshes used here (three nodes radially, twelve azimuthally) would give an indication of that accuracy, but the matrix used to solve the flow problem could no longer be stored in core on the CDC Cyber 74 machine used for these computations. A frontal equation solver such as that developed by Hood (1976) would be better suited to external storage of the flow matrix than the band solver used here.

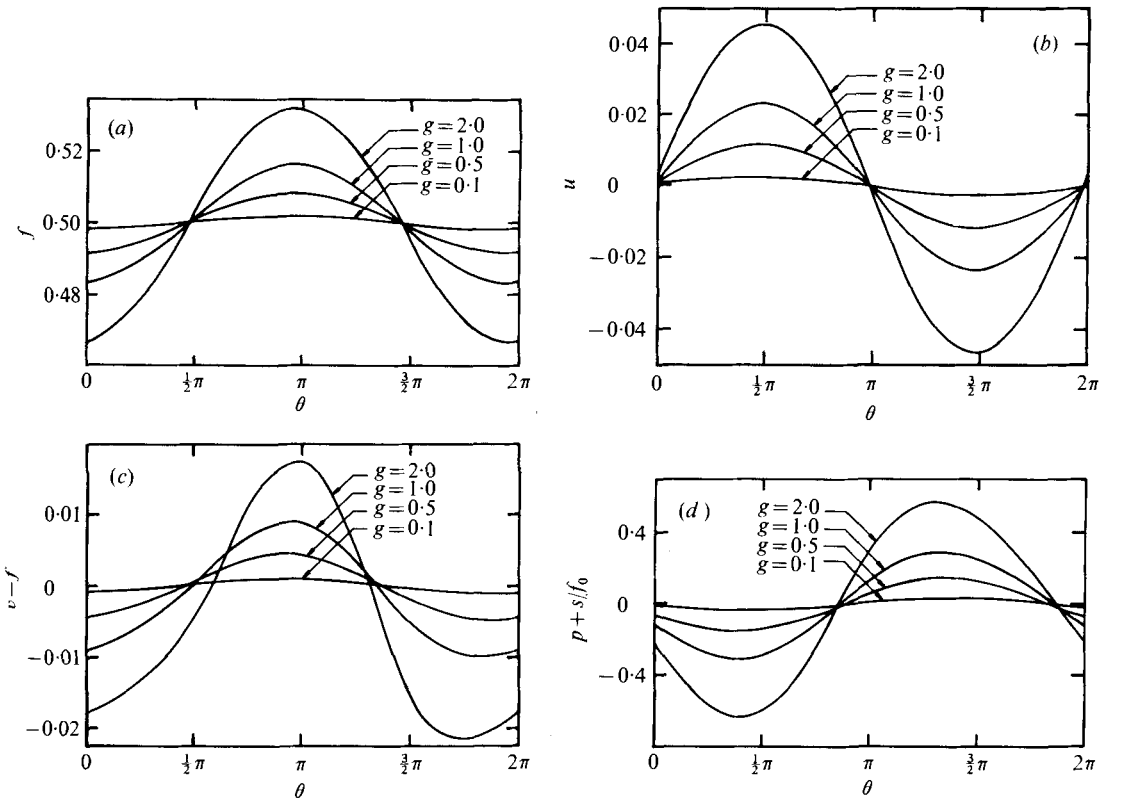

FIGURE 4. Effect of increasing gravity on (*a*) the free-surface location f, (*b*) the free-surface radial velocity u, (*c*) the deviation $v-f$ of the free-surface azimuthal velocity from solid-body rotation and (*d*) the liquid pressure $p+s/f_0$ at the free surface. $Re = 1$, $s = 1$, $f_0 = 0{\cdot}5$.

Sample solutions

Solutions for a selection of parameter sets were found in order to validate the numerical solutions and to test the effect of varying each of the parameters. Figure 3 is a map of the parameter space explored. The horizontal axes are the Reynolds number and gravity parameter and the vertical axis is the surface-tension parameter. Solid points indicate solutions for a liquid loading $f_0 = 0{\cdot}5$, i.e. the meniscus is on the average at half the cylinder radius. Open points are solutions for a lighter loading given by $f_0 = 0{\cdot}8$. The parameter sequence used to obtain the solutions is indicated by the arrows between neighbouring points. Broken arrows mean that the zero-gravity solution, i.e. solid-body rotation, was used as the initial guess. The encircled number accompanying the arrow is the number of iterations required to reduce the incremental change in surface location to less than 10^{-5}. The decimal number accompanying each solution point is the maximum deviation of the free-surface location from the average free-surface radius, i.e. $|f-f_0|$. This deviation is a good indicator of corresponding departures in the velocity and pressure fields.

From figure 3 it is plain that increasing deviation from solid-body rotation is caused, as expected, by increasing the Reynolds number or the gravity parameter, or decreasing the surface-tension parameter. The number of iterations to convergence

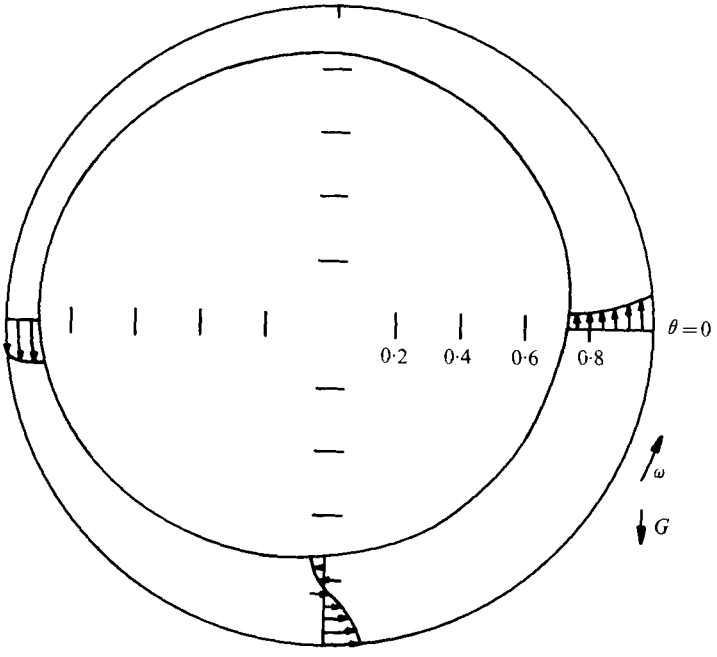

FIGURE 5. Free-surface location when $g = 0{\cdot}5$, $Re = 150$, $s = 1$ and $f_0 = 0{\cdot}8$. On the ascending side the azimuthal velocity lags the cylinder and on the descending side it leads, owing to gravitational acceleration. At the bottom ($\theta \sim \frac{3}{2}\pi$) a small region of recirculation has appeared.

depends not only on the size of a given parameter change but also on the values of the other parameters.

The effect of varying the gravity parameter with the other parameters held fixed can be seen in figure 4. The deviation of the meniscus location from the circle in solid-body rotation increases steadily as the gravity parameter increases, as shown in figure 4(*a*). As the circular meniscus shifts off concentricity (and begins to deform) the radial velocity at the free surface must also depart from zero, and that departure is shown in figure 4(*b*). The free-surface radial velocity changes sign when the film attains its minimum and maximum thicknesses. The departure of the free-surface azimuthal velocity from solid-body rotation is shown in figure 4(*c*). For the low Reynolds number case shown here, the departures are small, though it is clear that the liquid alternately lags and leads the cylinder on the ascending and descending sides of the domain as gravity alternately decelerates and accelerates the flow. Figure 4(*d*) shows the effect of gravity on the liquid pressure at the free surface. As expected, the pressure field is more sensitive to changes in gravity than are the velocity fields, though this sensitivity clearly depends on the size of the surface-tension parameter (the Weber number), since it is the surface tension which transmits the curvature of the surface to the pressure field. This transmission is represented in the normal-stress boundary condition (4.5).

It can be seen in figure 4 that there are progressively greater departures from the symmetry of solid-body rotation as the effect of gravity increases. The same is true as the Reynolds number increases and non-centripetal accelerations grow. An increase in the Reynolds number with the other parameters fixed corresponds to a reduction in

r†	θ	$df/d\theta$†	u	$\partial u/\partial r$	$\partial u/\partial\theta$	v	$\partial u/\partial r$	$\partial v/\partial\theta$	p	$\partial p/\partial r$	$\partial p/\partial\theta$
0·3824	0	0·0758	0·0709	−0·9520	0·2915	0·4052	−0·1558	0·5426	−2·0947	0·3750	−0·9112
0·6912	−0·1309	—	−0·0333	0·1811	0·1449	0·4744	1·1938	−0·1577	−1·9672	0·8032	−0·2877
1·0000	−0·2618	—	0	−0·0506	0·0813	1·0000	2·0172	−0·0137	−1·6992	1·7572	−0·3247
0·4350	0·5236	0·1269	0·1720	−1·7074	0·2529	0·5325	0·2783	0·7812	−2·1240	0·5865	−1·9800
0·7175	0·3927	—	−0·0179	−0·0098	0·2336	0·4909	0·9820	−0·0191	−2·0281	0·3281	−0·5130
1·0000	0·2618	—	0	−0·1333	0·1640	1·0000	2·4565	0·0441	−1·8746	1·2067	−0·1199
0·5088	1·0472	0·1577	0·2302	−2·2044	−0·1286	0·6115	1·2518	0·8512	−2·1487	1·5505	−3·1118
0·7544	0·9163	—	0·0134	−0·3813	0·3059	0·5458	0·9028	0·2327	−2·0456	−0·3204	−0·6104
1·0000	0·7854	—	0	−0·2375	0·2636	1·0000	2·8088	0·1635	−1·9965	0·1564	0·0527
0·5858	1·5708	0·1420	0·2125	−1·8717	−0·7520	0·6508	2·3485	0·6127	−2·1111	2·8341	−3·8405
0·7929	1·4399	—	0·0449	−0·7724	0·3506	0·6508	1·0168	0·4892	−2·0030	−0·8170	−0·5035
1·0000	1·3090	—	0	−0·2442	0·3100	1·0000	2·7769	0·2987	−2·0026	−0·8545	0·0424
0·6381	2·0944	0·0705	0·1337	−0·6767	−0·8984	0·6649	2·7561	0·1990	−2·0011	2·6432	−2·8791
0·8191	1·9635	—	0·0433	−0·7488	0·2831	0·7844	1·1324	0·4747	−1·9305	−0·9245	−0·0507
1·0000	1·8326	—	0	0·0309	0·2125	1·0000	1·8353	0·3378	−1·9090	1·1331	−0·2068
0·6438	2·6180	−0·0376	−0·0158	0·8930	−0·0952	0·5853	2·1489	−0·2269	−1·8849	0·0123	−0·4744
0·8219	2·4871	—	0·0097	−0·1260	−0·0191	0·8788	1·2882	0·0853	−1·8971	−0·3989	0·6005
1·0000	2·3562	—	0	0·3424	−0·0100	1·0000	0·2476	0·2948	−1·8050	−0·4400	−0·5412
0·5993	3·1416	−0·1290	−0·1084	1·2142	0·6913	0·3308	1·9244	−0·4267	−1·8532	−1·5943	0·9389
0·7997	3·0107	—	−0·0136	0·4377	−0·3204	0·8574	1·9189	−0·2904	−1·8858	0·4223	0·7997
1·0000	2·8798	—	0	0·2062	0·1683	1·0000	−0·4626	0·2727	−1·7102	0·5670	−0·4962
0·5236	3·6652	−0·1590	−0·0617	0·3848	0·6277	0·0952	1·6301	−0·3766	−1·8987	−1·2172	1·1359
0·7618	3·5343	—	−0·0180	0·4346	−0·3537	0·7443	2·4681	−0·1871	−1·8553	0·7777	0·6206
1·0000	3.4034	—	0	0·0500	−0·1391	1·0000	−0·2463	0·1735	−1·6031	1·0787	−0·1654
0·4465	4·1888	−0·1349	−0·0088	−0·1961	0·3508	−0·0018	0·9626	−0·2237	−1·9580	−0·6378	1·0459
0·7232	4·0579	—	−0·0214	0·2949	−0·2766	0·6345	2·4836	−0·1408	−1·8281	0·8085	0·4539
1·0000	3·9270	—	0	0·0240	−0·0667	1·0000	0·1894	0·0964	−1·4994	1·2301	−0·0219
0·3892	4·7124	−0·0855	−0·0099	−0·3303	0·1773	0·0058	0·5124	0·0054	−2·0085	−0·2487	0·9615
0·6946	4·5815	—	−0·0281	0·2579	−0·1728	0·5598	2·1376	−0·1530	−1·8193	0·7806	0·3447
1·0000	4·4506	—	0	0·0038	−0·0343	1·0000	0·6422	0·0615	−1·4400	1·2685	−0·1021
0·3592	5·2360	−0·0313	−0·0281	−0·2871	0·1325	0·0982	0·2186	0·1837	−2·0481	0·1408	0·6891
0·6796	5·1051	—	−0·0354	0·2707	−0·0615	0·5114	1·7787	−0·1903	−1·8413	0·8574	0·2043
1·0000	4·9742	—	0	−0·0023	−0·0049	1·0000	1·0981	0·0182	−1·4517	1·4511	−0·2838
0·3570	5·7596	0·0219	−0·0069	−0·4371	0·1949	0·2470	−0·0727	0·3313	−2·0752	0·3817	0·0361
0·6785	5·6287	—	−0·0378	0·2565	0·0439	0·4830	1·4681	−0·2037	−1·8955	0·9445	−0·0208
1·0000	5·4978	—	0	−0·0107	0·0301	1·0000	1·5619	−0·0159	−1·5428	1·7396	−0·3956

† Points (r,θ) for which values of $df/d\theta$ are given lie on the free surface.

TABLE 1. Numerical solution for $g = 0{\cdot}5$, $Re = 30$, $s = 1$ and $f_0 = 0{\cdot}5$.

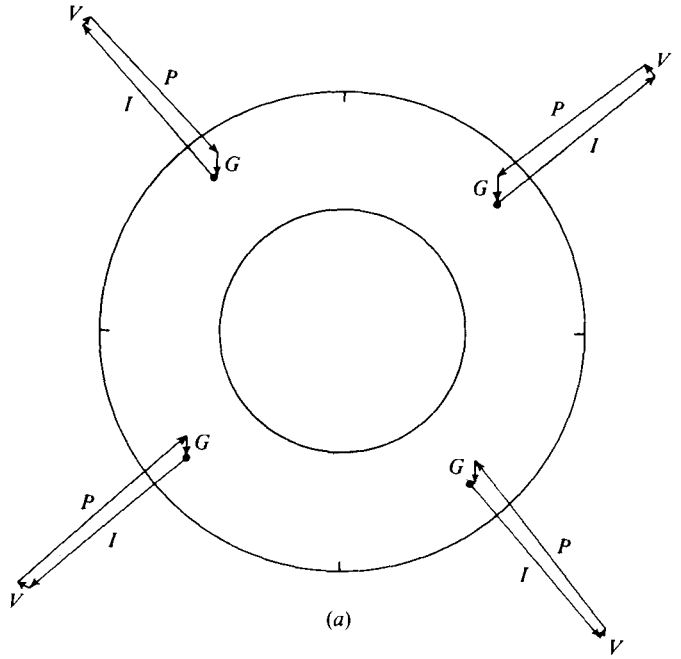

FIGURE 6. Local force estimates and free-surface location for $s = 1$ and $f_0 = 0{\cdot}5$. (*a*) $g = 0{\cdot}01$, $Re = 1$. (*b*) $g = 0{\cdot}5$, $Re = 30$. The vectors are the gravitational force G, the inertial force I, the pressure force P and the viscous force V.

the liquid viscosity. The maximum film thickness increases with Re and correspondingly the minimum film thickness decreases, the radial velocities grow, and the azimuthal velocities lead and lag the rim velocity by greater amounts. Where the Reynolds number and gravity parameter are sufficiently large, the azimuthal velocity may actually become negative, as shown in figure 5. A zone of recirculation has appeared at the bottom of the cylinder. The onset of recirculation is found to depend on the amount of liquid present: recirculation appears at lower Reynolds number for heavier liquid loading as indicated in figure 3. The flow sketched in figure 6 (*b*) contains a small recirculation zone and corresponds to the point just beyond the onset of recirculation for $f_0 = 0{\cdot}5$ in figure 3. Detailed numerical results for this case appear in table 1. Another case is tabulated in Orr (1976), and further results are available from the authors.

Another test of the validity of the numerical solutions can be made by comparison with a theoretical prediction of the behaviour of the maximum film thickness with increasing Reynolds number (Ruschak & Scriven 1976). The solution for $g \to 0$ predicts that the maximum film thickness always occurs in the upper right quadrant: for low Reynolds number the maximum thickness in near $\theta = 0$, whereas for large Reynolds number it approaches $\theta = \frac{1}{2}\pi$ (the minimum thickness is always diametrically opposite the maximum). The numerical solutions, however, accord with this prediction only when the surface-tension parameter s is small. When s is not small, exactly the opposite movement of the position of the maximum is observed, even at low gravity. That is, as the Reynolds number increases, the maximum descends into the lower right quadrant; moreover the maximum and minimum shift away from diametrical opposition. The reason for this disagreement between the asymptotic and numerical solutions lies in the fact that the free-surface perturbations at first order do not change the curvature of the meniscus, so that surface tension does *not* appear in the *asymptotic* solution at first order. The range of adequacy of the asymptotic solution is smaller the larger the Weber number and the surface tension. The effect is again the interaction of surface tension and meniscus curvature in the capillary-pressure term of the normal-stress boundary condition. When the meniscus departs appreciably from circularity, as when the Reynolds number and gravity parameter are not small, the presence of surface tension can substantially alter the flow.

Finally, it is of interest to compare the relative contributions of viscous, gravitational, pressure and inertial terms in the Navier-Stokes equation, and the contributions of curvature, viscous-stress and pressure terms in the normal-stress boundary condition. The gravitational term is known. Estimates of the inertial force I, pressure force P and viscous force V can be computed from a finite-element solution by evaluating the terms of an integral momentum balance on each element. For an interior element with boundary ∂E on which the normal is $\mathbf{n}$ the estimates are

$$\mathbf{I} = -\int_{\partial E} \mathbf{n}.\mathbf{v}\mathbf{v}ds, \quad \mathbf{P} = -\int_{\partial E} \mathbf{n}.p\mathbf{I}ds, \tag{6.1), (6.2}$$

$$\mathbf{V} = \int_{\partial E} \mathbf{n}.[\nabla\mathbf{v} + (\nabla\mathbf{v})^{\mathrm{T}}]ds. \tag{6.3}$$

If there is no gravity, the viscous term is zero while the inertial term consists solely of the centrifugal force, which is directed radially, and is exactly balanced by the

opposing pressure-gradient term. With small gravity, the viscous contribution remains small and the inertial and pressure-gradient forces have small azimuthal components. Figure 6(*a*) shows the free-surface location and force estimates for such a case ($g = 0{\cdot}01$, $Re = 1$, $s = 1$, $f_0 = 0{\cdot}5$). When gravity and the Reynolds number are larger the force balance becomes much more complex, as portrayed in figure 6(*b*) ($g = 0{\cdot}5$, $Re = 30$, $s = 1$, $f_0 = 0{\cdot}5$). For a typical element in the upper right quadrant the pressure-gradient force is small while gravity and the viscous force balance the inertial force. The forces do not quite balance because the solutions used to evaluate them are approximate; also, the viscous force terms require derivatives of the solutions, which are less accurate than the solutions themselves. In an element in the upper left quadrant a larger inertial force balances a larger pressure force and a viscous force which has changed direction, in agreement with the fact that the azimuthal velocity leads the rim velocity on the descending side. In the lower right quadrant viscous forces are small. It is obvious that all of the terms in the Navier–Stokes equation are important for this flow. Similar estimates of the capillary pressure, normal viscous stress and pressure jump in the normal-stress boundary condition confirm that all the terms are generally of comparable size in rimming flows that depart appreciably from solid-body rotation.

Conclusion

The results presented here represent an advance in numerical simulation of viscous free-surface flows with surface tension. They are also a considerable extension of the finite-element method beyond previous applications by Chan & Larock (1973), Larock & Taylor (1976), Nickell *et al.* (1974) and Thompson *et al.* (1969), none of which included surface tension and in all of which the flow was idealized as either creeping or inviscid. The full Navier–Stokes equation for steady, two-dimensional, incompressible flow is solved here, and the effect of surface tension is fully accounted for in the normal-stress boundary condition.

The solutions, samples of which are reported here, are clearly the result of complex interaction of inertial, gravitational, pressure, viscous and capillary forces, none of which can be disregarded except in limiting cases. It is apparent that other nonlinear flows of this degree of complexity can be simulated by the method presented, that more irregular free-surface flow domains can also be handled, and that the finite-element solutions will be convenient representations for further analyses of transport and stability.

This work was supported in part by the National Science Foundation. The authors are grateful to the University Computer Center, University of Minnesota for a grant of computer time and to H. F. Weinberger for discussions of the existence of solutions to nonlinear problems.

REFERENCES

Chan, S. T. K. & Larock, B. E. 1973 Fluid flows from axisymmetric orifices and valves. *J. Hydr. Div., Proc. A.S.C.E.* **99**, 81–97.

Deiber, J. A. & Cerro, R. L. 1976 Viscous flow with a free surface inside a horizontal rotating drum. *Ind. Engng Chem. Fund.* **15**, 102–110.

Douglas, J. & Dupont, T. 1973 A finite element collocation method for quasilinear parabolic equations. *Math. Comp.* **27**, 17–28.

DUSSAN V., E. B. & DAVIS, S. H. 1974 On the motion of a fluid–fluid interface along a solid surface. *J. Fluid Mech.* **65**, 71–95.

GREENSPAN, H. P. 1976 On a rotational flow disturbed by gravity. *J. Fluid Mech.* **74**, 335–351.

HOOD, P. 1976 Frontal solution program for unsymmetric matrices. *Int. J. Numer. Meth. Engng* **10**, 379–399.

HOOD, P. & TAYLOR, C. 1974 Navier–Stokes equations using mixed interpolation. In *Finite Element Methods in Flow Problems* (ed. J. T. Oden, O. C. Zienkiewicz, R. H. Hallagher & C. Taylor), pp. 121–132. University of Alabama Press, Huntsville.

HUH, C. 1969 Capillary hydrodynamics: interfacial instability and the solid/liquid/fluid contact line. Ph.D. thesis, University of Minnesota.

HUH, C. & SCRIVEN, L. E. 1971 Hydrodynamic model of steady movement of a solid/liquid/fluid contact line. *J. Colloid Interface Sci.* **35**, 85–99.

LAROCK, B. E. & TAYLOR, C. 1976 Computing three-dimensional free surface flows. *Int. J. Numer. Meth. Engng* **10**, 1143–1152.

NICKELL, R. E., TANNER, R. I. & CASWELL, B. 1974 The solution of viscous incompressible jet and free-surface flows using finite-element methods. *J. Fluid Mech.* **65**, 189–206.

ODEN, J. T. 1972 *Finite Elements of Nonlinear Continua.* McGraw-Hill.

ORR, F. M. 1976 Numerical simulation of viscous flow with a free surface. Ph.D. thesis, University of Minnesota.

ORR, F. M., BROWN, R. A. & SCRIVEN, L. E. 1977 Three-dimensional menisci: numerical simulation by finite elements. *J. Colloid Interface Sci.* **60**, 137–147.

ORR, F. M., SCRIVEN, L. E. & RIVAS, A. P. 1975 Menisci in arrays of cylinders: numerical simulation by finite elements. *J. Colloid Interface Sci.* **52**, 602–610.

PHILLIPS, O. M. 1960 Centrifugal waves. *J. Fluid Mech.* **7**, 340–352.

RUSCHAK, K. J. 1974 The fluid mechanics of coating flows. Ph.D. thesis, University of Minnesota.

RUSCHAK, K. J. & SCRIVEN, L. E. 1976 Rimming flow of liquid in a rotating horizontal cylinder. *J. Fluid Mech.* **76**, 113–125.

STRANG, G. & FIX, G. 1973 *An Analysis of the Finite Element Method.* Prentice-Hall.

STROUD, A. H. 1971 *Approximate Calculation of Multiple Integrals.* Prentice-Hall.

TANNER, R. I., NICKELL, R. E. & BILGER, R. W. 1975 Finite element methods for the solution of some incompressible non-Newtonian fluid mechanics problems with free surfaces. *Comp. Meth. Appl. Mech. Engng* **6**, 155–174.

TAYLOR, G. I. 1963 Cavitation of a viscous fluid in narrow passages. *J. Fluid Mech.* **16**, 595–619.

THOMPSON, E. G., MACK, L. R. & LIN, F. S. 1969 Finite element method for incompressible slow viscous flow with a free surface. *Dev. in Mech.* **5**, 93.

WEATHERBURN, C. E. 1939 *Differential Geometry*, vol. 1. Cambridge University Press.

WILLIAMSON, A. S. 1970 Tearing separation of viscous fluid layers under surface tension membrane boundaries. Ph.D. thesis, Stanford University.

WILLIAMSON, A. S. 1972 The tearing of an adhesive layer between flexible tapes pulled apart. *J. Fluid Mech.* **52**, 639–656.

ZLÁMAL, M. 1970 A finite element procedure of the second order of accuracy. *Numer. Math.* **14**, 394–402.

ZLÁMAL, M. 1973*a* The finite element method in domains with curved boundaries. *Int. J. Numer. Meth. Engng* **5**, 367–373.

ZLÁMAL, M. 1973*b* Curved elements in the finite element method. *SIAM J. Numer. Anal.* **10**, 229–240.